Electronic Supplementary Material (ESI) for Journal of Materials Chemistry A.
This journal is © The Royal Society of Chemistry 2024

Phase-pure Ruddlesden-Popper Tin Halide Perovskites for Solar Energy Conversion Application

Han Pan [a*], Yilin Wang [a], Yong Zheng [a], Shufang Gao [a], Yan Xiong [a], Shubo Cheng [a], Nian Chen [a], Wenxing Yang [a] *, Xiu Gong [b], Jibin Zhang [c], Yan Shen [d] and Mingkui Wang [d] *

[a] School of Physics and Optoelectronic Engineering, Yangtze University, Jingzhou 434023, P.R. China

[b] College of Physics, Guizhou Province Key Laboratory for Photoelectrics Technology and Application, Guizhou University, Guiyang 550025, P.R. China

[c] Key Laboratory of Materials Physics of Ministry of Education, School of Physics and Microelectronics, Zhengzhou University, Daxue Road 75, Zhengzhou, 450052 China

[d] Wuhan National Laboratory for Optoelectronics, School of Optoelectronic Science and Engineering, Huazhong University of Science and Technology, Wuhan 430074, P.R. China

Experimental Section

SnI_2 (99.999%), hydroiodic acid (57 wt.% in H_2O, distilled, stabilized, 99.95%), hypophosphorous acid solution (50 wt.% in H_2O) and formamidinium iodide (≥99%, anhydrous) were purchased from Sigma-Aldrich and used as received. Benzylamine (99%) and 2,4-Difluorobenzylamine (98%) were purchased from Aladdin and used as received.

Synthesis of BEI and FBEI: hydroiodic acid (12.3 g, 0.055 mol) reacted with benzylamine (5.3 g, 0.05 mol.) for 2 hours under ice bath. The crude product was separated out by evaporating the solvent under reduced pressure. White crystals were obtained after washed with diethyl ether, recrystallized in ethanol and drying at 60 °C overnight in a vacuum. FBEI was prepared using the same method, only changed the benzylamine to 2,4-difluorobenzylamine.

The perovskite precursor solutions were prepared by mixing BEI or FBEI, FAI, SnI_2 and SnF_2 in anhydrous in DMF and DMSO (volume ratio is 4:1) with a molar ratio of 2:3:4:0.1. The concentration of $(BE)_2FA_3Sn_4I_{17}$ and $(FBE)_2FA_3Sn_4I_{17}$ is 0.1 M. The mixture solutions were stirred for 2h in N_2 glove box.

Device fabrication

The ITO glass was sequentially cleaned with detergent, deionized water, acetone and ethanol, and then treated in UV-ozone for 30 min. A 40 nm thick PEDOT:PSS (Baytron PVP Al 4083) was spin-coated onto the ITO substrate at 4500 rpm for 40 s and annealed at 140 °C for 10 min in air. After perovskite films were spin-coated at 4000 rpm for 60 s and then annealed on 60 °C for 10 seconds and post on 100 °C for 10 minutes, PC61BM (20 $mg \cdot mL^{-1}$ in chlorobenzene) and BCP (0.5 $mg \cdot mL^{-1}$ in isopropanol) were sequentially coated at 2000 rpm for 40 s and 4000 rpm for 40 s, respectively. Finally, 100 nm Ag was deposited by thermal evaporation.

Characterization

XRD measurements were performed with a Shimadzu XRD-6100 diffractometer with Cu Kα radiation. The surface morphology of films were characterized with FEI Nova Nano SEM 450. The crystallization process of perovskite films fabricated from the solutions were recorded by optical microscope (Olympus BX51). Visible absorption spectra were recorded using a PerkinElmer Lambda1050 spectrophotometer. The steady-state photoluminescence (PL) spectrum was measured using Horiba Jobin Yvon system with an excitation laser beam at 532 nm and a repetition rate of 76 MHz. The time-resolved luminescence decays were obtained with time-correlated single photo counting system (PicoHarp 300, PicoQuant GmbH). The excitation light source was Ti:Sapphire laser (Mira 900, Coherent; 76 MHz, 130 fs). The photocurrent-voltage (J-V) characteristics solar cells were obtained by a Keithley model 2400 digital source meter. A xenon light source solar simulator (450 W, Oriel, model 9119) with AM 1.5G filter (Oriel, model 91192) was used to give an irradiance of 100 mW cm-2 at the surface of the solar cells. The incident photon conversion efficiency (IPCE) measurement was obtained with alternating current (AC) model (130 Hz). The dynamic light scattering and zeta potential measurement of the perovskite precursor solutions were measured using Brookhaven 90Plus Particle Size and PALS Zeta Potential Analyzer.

Measurements

The molecular dynamics simulations were performed using the GRMOACS 2020.6 package [1]. The Visualization of structures were performed by VMD software [2]. The molecular were mixed in a cubic box with periodic boundary conditions by using PACKMOL package [3]. The number of the molecular is shown in the following table.

System/molecular	1	2	4	3	DMSO	DMF
1	20	\	\	\	281	1037
2	\	20	\	\	281	1037

3	\	\	20	\	281	1037
4	\	\	\	20	281	1037

The Amber Force Field [4] was selected in this work, which is good for investigation of various small organic molecules [5]. The ACPYPE [6] code was used to generate the desired force field parameters for the Sorbitol and Choline chloride.

Before starting MD simulation, the initial configurations were relaxed using a conjugate gradient minimization scheme. The step size was 0.01 nm, and the cycle was set to 5000 steps. The minimization was considered to have converged when the minimum force was less than 50 $kJ \cdot mol^{-1} \cdot nm^{-1}$. The van der Waals interaction was calculated by the cut-off method, atomic electrostatic interaction was calculated by PME (particle mesh Ewald), and both the cut-off and PME distances were 1.0 nm [7]. Then, the system was equilibrated with a pressure of 1.0 bar to achieve a desired density. The Berendsen and V-rescale methods were used to control the pressure and temperature. The time constant was 1.0 ps, and the compressibility was 4.5×10^{-5} bar^{-1}. The equilibrium was 5 ns for all systems with a 0.001 ps time step. Finally, the production ran for 50 ns. The pressure control was changed to the Parrinello-Rahman method in the production run. In addition, the LINCS (Linear Constrain Solver) algorithm [8]was used to impose constraints on the hydrogen bond.

Calculations Methods. DFT calculations were performed using Vienna Ab initio Simulation Package based on density functional theory. The exchange-correlation energy was described using the revised Perdew-Burke-Ernzerhof exchange-correlation density functional (PBE) within the generalized-gradient approximation (GGA). An energy cutoff of 400 eV and a k-point mesh of $2 \times 2 \times 1$ are used for geometry optimization. The structures were fully optimized via total energy minimization, with the total energy converged to less than 10^{-4} eV.

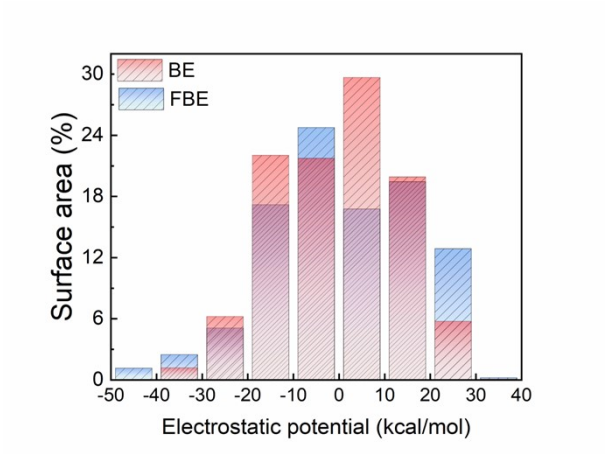

Figure S1. Surface area in each electrostatic potential range of BE and FBE.

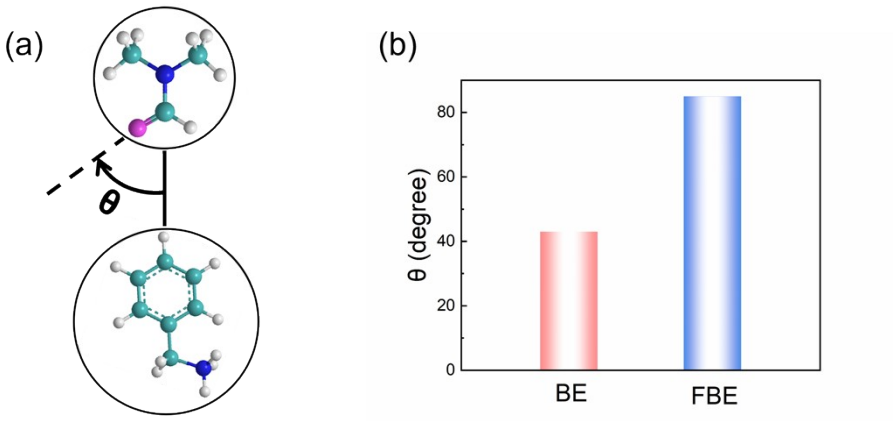

Figure S2. (a) Schematic representation of the DMF orientation near the terminal benzyl of spacer cations. (b) Maximum probable solvent orientation from the terminal benzyl of spacer cations.

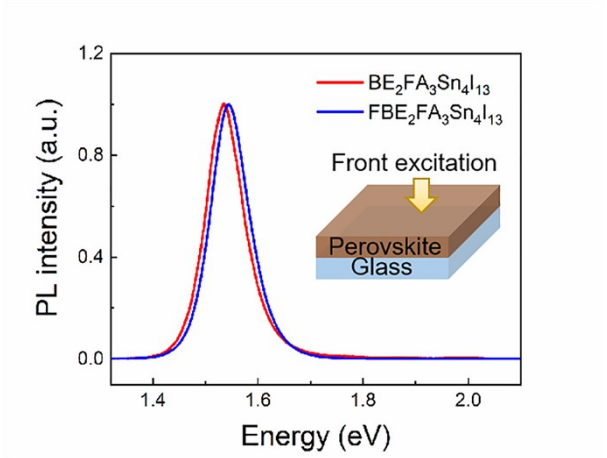

Figure S3. Steady-state PL spectra of the $BE_2FA_3Sn_4I_{13}$-based and $FBE_2FA_3Sn_4I_{13}$-based films from the front side.

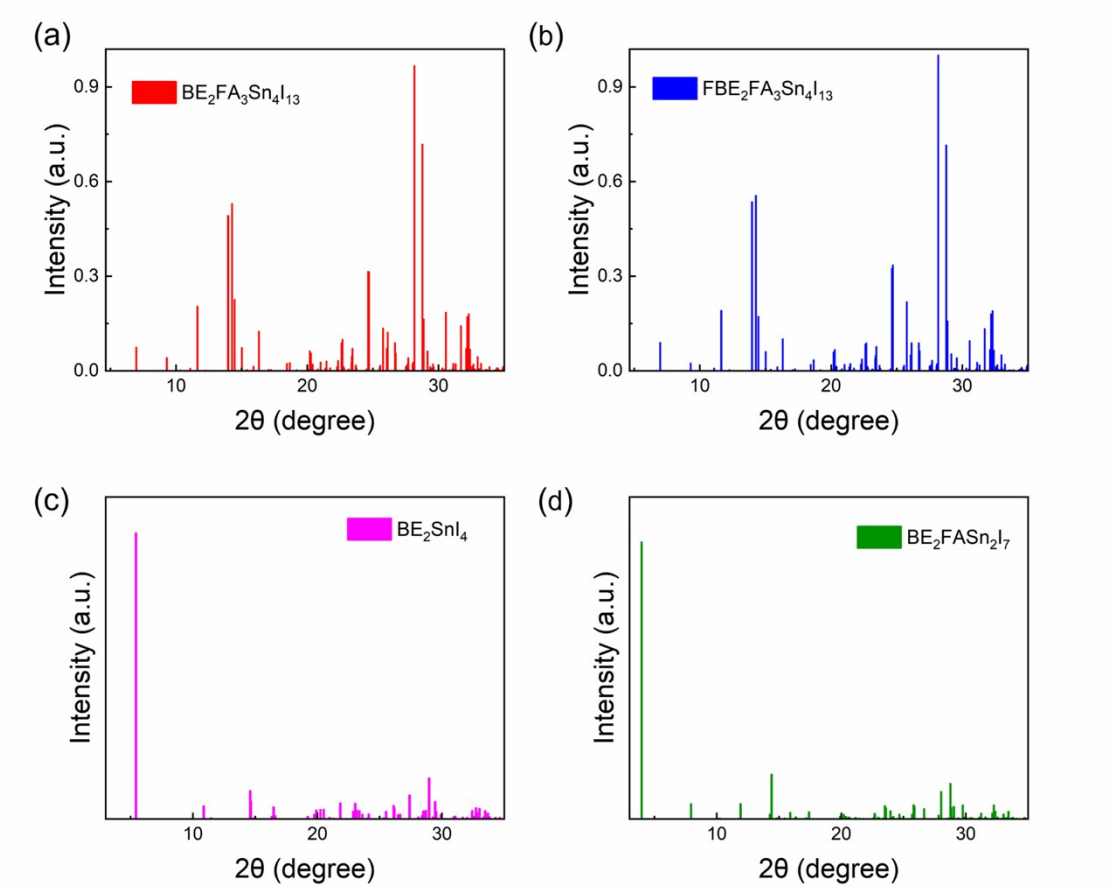

Figure S4. Calculated powder XRD patterns of (a) the $BE_2FA_3Sn_4I_{13}$-based, (b) $FBE_2FA_3Sn_4I_{13}$-based, (c) the BE_2SnI_4-based and (d) the $BE_2FASn_2I_7$-based perovskites.

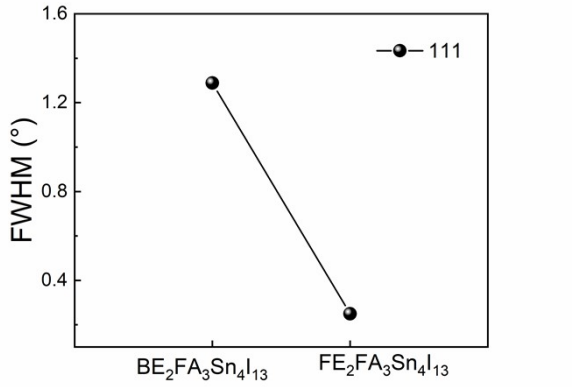

Figure S5. The full width at half maximum (FWHM) of the $BE_2FA_3Sn_4I_{13}$-based and $FBE_2FA_3Sn_4I_{13}$-based films pertaining to the major peak (111).

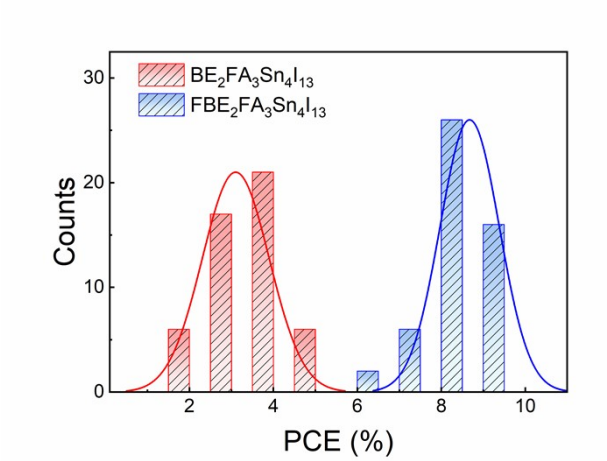

Figure S6. The PCE histogram of 50 devices based on $BE_2FA_3Sn_4I_{13}$ and $FBE_2FA_3Sn_4I_{13}$ perovskites.

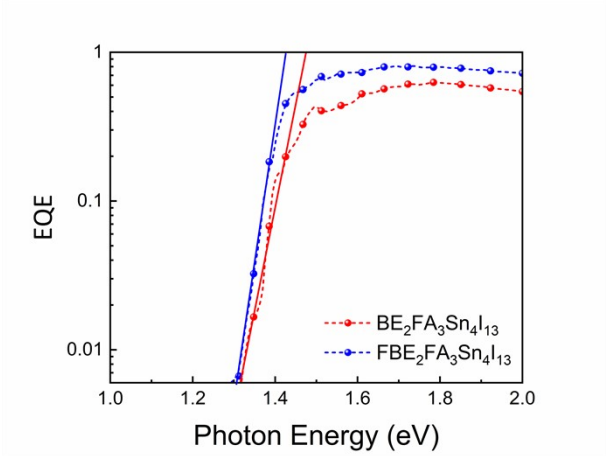

Figure S7. Semi-log plot of EQE values versus photon energy of the $BE_2FA_3Sn_4I_{13}$-based and $FBE_2FA_3Sn_4I_{13}$-based devices.

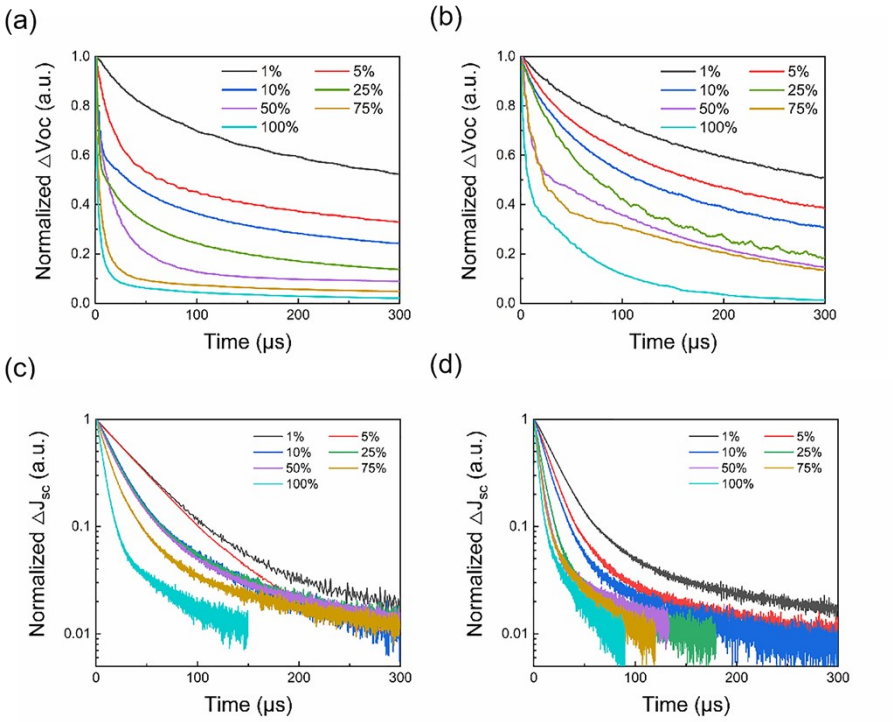

Figure S8. Transient photovoltage of a) $BE_2FA_3Sn_4I_{13}$-based and b) $FBE_2FA_3Sn_4I_{13}$-based devices under varying light intensity. Transient photocurrent of c) $BE_2FA_3Sn_4I_{13}$-based and d) $FBE_2FA_3Sn_4I_{13}$-based devices under varying light intensity.

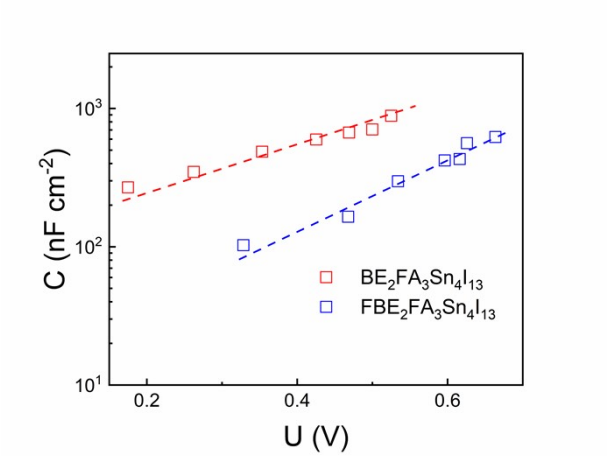

Figure S9. Capacitance of the $BE_2FA_3Sn_4I_{13}$-based and $FBE_2FA_3Sn_4I_{13}$-based devices.

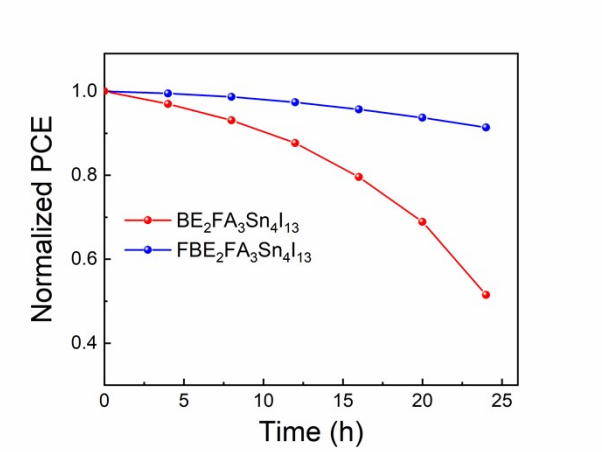

Figure S8. Normalized PCEs versus time for the $BE_2FA_3Sn_4I_{13}$-based and $FBE_2FA_3Sn_4I_{13}$-based devices.

Table S1. The photovoltaic parameters of the $BE_2FA_3Sn_4I_{13}$-based and $FBE_2FA_3Sn_4I_{13}$-based devices.

Device	*V*oc (V)	*J*sc (mA cm^{-2})	FF (%)	PCE (%)
$BE_2FA_3Sn_4I_{13}$	0.56	15.17	48.6	4.13
$FBE_2FA_3Sn_4I_{13}$	0.69	21.10	63.5	9.25

References:

[1] M. Abraham, T. Murtola, R. Schulz, S. Páll, J.C. Smith, B. Hess, E. Lindahl, SoftwareX, 2015, 1, 19-25.

[2] W. Humphrey, A. Dalke, K. Schulten, Journal of molecular graphics, 1996, 14(1), 33-38.

[3] L. Martínez, R. Andrade, E.G. Birgin, J. M. Martínez, Journal of computational chemistry, 2009, 30, 2157-2164.

[4] J. Wang, R. M. Wolf, J.W. Caldwell, P.A. Kollman, D.A. Case, Journal of computational chemistry, 2004, 25, 1157-1174.

[5] P. Han, W. Nie, G. Zhao, P. Gao, Journal of Molecular Liquids, 2022, 366, 120243.

[6] D. Sousa, W. Vranken, BMC research notes, 2012, 5: 1-8.

[7] P. Li, B. Roberts, D. Chakravorty, K. Merz, Journal of chemical theory and computation, 2013, 9, 2733-2748.

[8] B. Hess, H. Bekker, H. Berendsen, J. Fraaije, Journal of computational chemistry, 1997, 18(12): 1463-1472.